

Article

Properties of Barium Ferrite Nanoparticles and Bacterial Cellulose-Barium Ferrite Nanocomposites Synthesized by a Hydrothermal Method

Chanagan Tanakulrungsarit^{1,a}, Wiyada Mongkolthanaruk^{2,b}, Sampo Tuukkanen^{3,c}, and Supree Pinitsoontorn^{1,4,*}

1 Materials Science and Nanotechnology Program, Department of Physics, Faculty of Science, Khon Kaen University, Khon Kaen 40002, Thailand

2 Department of Microbiology, Faculty of Science, Khon Kaen University, Khon Kaen 40002, Thailand

3 Faculty of Medicine and Health Technology (MET), Tampere University (TAU), Tampere FI-33101, Finland

4 Institute of Nanomaterials Research and Innovation for Energy (IN-RIE), NANOTEC-KKU RNN on Nanomaterials Research and Innovation for Energy, Khon Kaen University, Khon Kaen 40002, Thailand
E-mail: ^at.chanagan@gmail.com, ^bwiymon@kku.ac.th, ^csampo.tuukkanen@tuni.fi, ^{d,*}psupree@kku.ac.th
(Corresponding author)

Abstract. Barium ferrite (BFO) is a class of hard magnetic materials which is technologically important for many applications. Likewise, bacterial cellulose (BC) is a natural cellulose with a unique nanostructure and properties. Particularly, magnetic BC membrane, produced by incorporation of magnetic nanoparticles (NPs) in the BC structure, has recently been a research focus of many research groups. In this work, BFO NPs and BC/BFO nanocomposites were fabricated by hydrothermal synthesis. The BFO NPs could be fabricated only when the synthesis temperature reached 290 °C, with the faceted plate-like shape. Increasing the synthesis temperature gradually changed the magnetic properties from paramagnetic to superparamagnetic and ferromagnetic. Maximum M_s , M_r and H_c of 43 emu/g, 21 emu/g, and 1.6 kOe, respectively, were found. For BC/BFO nanocomposites, the hydrothermal synthesis conditions were limited by the stability of BC, i.e., 150 – 210 °C (for 1 h), or 1 – 7 h (at 190 °C). Using the higher temperature or time resulted in disintegration or decomposition of BC. It was found that very small NPs were coated on the BC nanofibers but the BFO phase was not observed by XRD. However, the magnetic measurement showed the hysteresis loops for the nanocomposites synthesized at 190 °C for 3 – 7 h. The observation of the hysteresis loops could be attributed to a small fraction of BFO in the nanocomposite that cannot be detected by XRD. The BC/BFO nanocomposite membranes were demonstrated for their magnetic attraction, flexibility, and lightness, which make them potential uses for flexible information storage or lightweight magnets.

Keywords: Barium ferrite, bacterial cellulose, magnetic, nanoparticles, nanocomposites, hydrothermal.

ENGINEERING JOURNAL Volume 25 Issue 10

Received 5 May 2021

Accepted 10 October 2021

Published 31 October 2021

Online at <https://engj.org/>

DOI:10.4186/ej.2021.25.10.95

This article is based on the presentation at The 7th KKU International Engineering Conference 2021 (KKU-IENC 2021) at Khon Kaen University, Khon Kaen, Thailand, 12th-14th May 2021.

1. Introduction

Magnetic materials can be classified into two types for applications: soft and hard magnetic phases. Soft magnetic materials exhibit high magnetic susceptibility, large saturation magnetization (M_s), narrow hysteresis loop, and small coercivity (H_c), whereas for hard magnetic materials, large M_s and magnetic remanence (M_r) with wide hysteresis loop and large H_c are required [1]. Amongst hard magnetic materials, hexagonal ferrites (M-type ferrites), such as strontium ferrite ($\text{SrFe}_{12}\text{O}_{19}$) or barium ferrite ($\text{BaFe}_{12}\text{O}_{19}$, BFO), have been studied extensively due to their outstanding hard magnetic properties and their applications in a wide range [2]. In particular, for BFO, there have been a number of research focusing on the synthesis and properties of BFO nanoparticles (NPs) and their nanocomposites. For instance, the BFO NPs, synthesized by a co-precipitation method, were doped with Zn, Co, and Zr cations to increase the magnetic and microwave absorption properties [3]. In another study, BFO/graphite nanocomposites were synthesized and applied as electromagnetic wave absorbers [4]. It was found that the electromagnetic waves absorption of the nanocomposites was enhanced from the combination of the dielectric loss from graphite and magnetic loss from ferrite. These nanocomposites showed a potential to be applied for stealth technology or military applications. On the other hand, Choudhary et al. fabricated Pb-doped BFO/ polyaniline-wax nanocomposites [5]. The resultant nanocomposites showed the improved efficiency in electromagnetic interference (EMI) shielding and the ability to control electromagnetic smog. Furthermore, the core-shell NPs were engineered from the BFO core and poly (3,4-ethylenedioxy thiophene) (PEDOT) shell [6]. This nanostructure improved the microwave absorption properties due to the high dielectric and magnetic losses of the core-shell structured NPs.

It is clearly seen that BFO NPs are very useful hard magnetic materials and their nanocomposites show various potential applications. Several synthetic polymers have been used as the matrix for the nanocomposites. However, the current trend of research tends to employ natural bioresources for maintaining environmental friendliness and sustainability. Cellulose is one of the most important and abundant natural polymers. It is an inexhaustible raw material and a key source of sustainable materials on an industrial scale [7]. Therefore, using cellulose as a matrix for fabrication of BFO nanocomposites is an interesting alternative. Particularly, bacterial cellulose (BC), a natural polymer produced by the cultivation of bacteria, exhibits unique structural features and intriguing properties. It consists of a three-dimensional nanostructure formed by a network of highly crystalline cellulose nanofibrils. It also possesses remarkable mechanical properties, high water absorbency, high moldability, biodegradability and excellent biological affinity [8-10]. Therefore, it is one of the excellent choices as a matrix for fabricating BFO nanocomposites.

BC composited with magnetic NPs have been explored with potential uses in medical and environmental applications, as well as in advanced electronic devices [11]. The most common magnetic NPs that have been incorporated into a BC nanostructure are limited to magnetite (Fe_3O_4) NPs or other soft magnetic phases [12-14]. These soft magnetic materials are desired for some applications, such as actuators, sensors, and heavy metal adsorption [15-20] but for other applications, e.g. information storage, anti-counterfeit, or permanent magnets, the hard magnetic properties are required. Therefore, the BC incorporated with hard magnetic NPs needs to be researched.

In this work, we therefore studied the properties of BFO NPs, and BFO nanocomposites using BC as the matrix. In literatures, BFO NPs could be chemically synthesized by several techniques, such as co-precipitation [3] or citrate-gel auto-combustion [21, 22]. However, to obtain the desired BFO phase, the NPs need to be fired at high temperature (>800 °C). Such high temperature is not applicable for the fabrication of BC/BFO nanocomposites because BC starts decomposed at the temperature above ~ 300 °C [12, 16]. Alternatively, hydrothermal synthesis is a technique that can produce single phase nanomaterials at relatively low temperature by the aid of high pressure [23]. It was used to synthesize BFO NPs without a need of high-temperature post-annealing [24]. Thus, it is a suitable method for preparing both BFO NPs and BC/BFO nanocomposites. The hydrothermally synthesized NPs and nanocomposites in this work were subjected to several characterization techniques to determine their crystal structures, morphologies, sizes, and magnetic properties.

2. Materials and Methods

2.1. Materials

The chemicals used in this work were iron (III) nitrate nonahydrate ($\text{Fe}(\text{NO}_3)_3 \cdot 9\text{H}_2\text{O}$, 99+%, ACROS Organics), barium nitrate ($\text{Ba}(\text{NO}_3)_2$, AR grade, Himedia), sodium hydroxide (NaOH , 99%, RCI Labscan), yeast extract powder (Himedia), D-Glucose (anhydrous AR, Ajax Finechem), and the bacterial strain *Komagataibacter nataicola* (strain TISTR 975), from the Microbiological Resources Centre, Thailand Institute of Scientific and Technological Research (TISTR).

2.2. BC Preparation

The process for preparing BC was adapted from [25]. In brief, BC was cultivated using the bacterial strain TISTR 975 in a liquid culturing medium consisting of 1 L of de-ionized (DI) water, 100 g of D-glucose, and 10 g of yeast extract powder. After agitated cultivation at 30 °C for 24 h, the cell suspension was transferred into a fresh culture medium, and then incubated at 30 °C under a static condition for 3 days. Thin BC pellicles were collected and purified in boiling DI water for 2 h. After that, BC pellicles

were soaked in 0.5 M of NaOH solution for 15 minutes, followed by soaking in 5 wt.% NaOH solution for 24 h. In the final step, the BC pellicles were washed in DI water until the color changed from brown to white, and the pH became neutral. They were then freeze-dried to obtain the BC aerogels.

2.3. Synthesis of BFO NPs and BC/BFO Nanocomposites

For the synthesis of $\text{BaFe}_{12}\text{O}_{19}$ (BFO) NPs, 7.867 g of $(\text{Fe}(\text{NO}_3)_3 \cdot 9\text{H}_2\text{O})$ and 1.574 g of $\text{Ba}(\text{NO}_3)_2$ were dissolved in 400 mL of DI water with continuous stirring until homogeneous solution was obtained. Then, 400 mL of 0.78 M NaOH was added and stirred rigorously for 30 min. The solution changed the color into red brown, which was then transferred to an autoclave for hydrothermal reaction. The temperature and the holding time for the hydrothermal synthesis were adjusted and systematically studied. The chemical reaction is according to the equation: $\text{Ba}(\text{NO}_3)_2 + 12 \text{Fe}(\text{NO}_3)_3 \cdot 9\text{H}_2\text{O} + 38 \text{NaOH} \rightarrow \text{BaFe}_{12}\text{O}_{19} + 38 \text{NaNO}_3 + 127 \text{H}_2\text{O}$. After the hydrothermal process, the precipitated powders were washed with acetic acid, and subsequently with water several times until the pH of 7 was reached. They were oven-dried at 60 °C before use or further characterization.

For fabricating BC/BFO nanocomposites, the BC aerogels were soaked in the $(\text{Fe}(\text{NO}_3)_3 \cdot 9\text{H}_2\text{O} + \text{Ba}(\text{NO}_3)_2)$ solution for 15 hours to allow the diffusion of Fe^{3+} and Ba^{2+} ions into the BC structure. The rest of the process was the same as for the BFO NPs hydrothermal synthesis. After the process, the BC was freeze-dried again to obtain the BC/BFO nanocomposite aerogels.

2.4. Characterization

The phase and crystal structure of the samples was determined using X-ray diffraction (XRD) with a diffractometer (PANalytical, Empyrean, USA) in the 2 θ range of 10 - 80°. A transmission electron microscope (TEM, FEI-Tecna G2 20, USA) was used to investigate the size and morphology of BFO NPs. The surface morphology of the BC/BFO nanocomposites were studied using a field emission scanning electron microscope (FESEM) (FEI, Helios, USA). Before imaging, the samples were gold coated to improve conductivity. Magnetic properties measurements were carried out using a vibrating sample magnetometer (VSM) option in the VersaLab instrument (Quantum Design, USA) with the maximum applied field of 30 kOe.

3. Result and Discussion

Figure 1(a) shows the XRD patterns of the synthesized NPs under different temperatures and holding times of the hydrothermal process, along with the reference pattern ($\text{BaFe}_{12}\text{O}_{19}$, ICDD: 00-039-1433). It is clearly seen that at the synthesis temperature ranging from 190 to 270 °C at the holding time of 1 h, the NPs do not

form the desired phase. It is implied that the synthesis conditions are not favorable for the formation of the BFO phase. On the other hand, for the synthesis temperature of 290 °C, the XRD pattern of the NPs (Fig. 1(b)) matches very well with most of the peaks from the standard BFO pattern. This indicates that the hydrothermal process at 290 °C can successfully synthesize the BFO NPs. Figure 1(b) also shows the XRD pattern of the NPs hydrothermally synthesized at 290 °C for different holding time (1 h, 3 h and 5 h). All samples show the XRD pattern corresponded to the standard peaks but prolonging the hydrothermal reaction time results in higher crystallinity of the samples.

To investigate the size and morphology of the NPs, the TEM study was carried out, and the results are presented in Fig. 2. For the samples synthesized at the temperature from 190 to 270 °C, the NPs exhibited spherical shapes with relatively small sizes in the range of 10 – 17 nm. The average size of the particles increases with hydrothermal temperature. Conversely, the NPs synthesized at 290 °C for 1-5 h show the facet plate-like shape with the much larger sizes (140 – 208 nm). The sizes of the plates also increased with the holding time. The changes between these two groups of samples are consistent with the XRD results. At the lower temperature (270 °C and below), the BFO phase was not formed so that the particles were mostly in the precursor stage, and thus, the sizes were small and in round shape. On the other hand, at 290 °C, the samples formed the BFO phase. Therefore, the morphology of the samples changed into facet plates and the sizes grew much larger.

The magnetic measurement results of the synthesized NPs are shown in Fig. 3. Figure 3(a) shows the M-H curve of the NPs synthesized at 190 – 270 °C. The M-H curve measures the responded magnetization (M) to the applied magnetic field (H). It can inform the magnetic behaviors of the samples, and several magnetic parameters can be extracted. For the relatively low hydrothermal temperature (190 and 210 °C), the samples show the almost linear relationship of M and H, implying a paramagnetic main phase of the samples. Increasing the synthesis temperature to 230 °C resulted in a slight S-shape curve, which infers superparamagnetism due to the nanosize of the particles. These results are well supported by the XRD and TEM analysis since the BFO phase was not formed at these temperatures, and thus the hard magnetic properties were not observed. Further increasing the hydrothermal temperature to 250 and 270 °C led to the appearance of M-H hysteresis loops, with low saturation magnetization (M_s) (1-2 emu/g), low magnetic remanence (M_r) (0.1-0.5 emu/g), and small coercivity (H_c). The existence of the M-H loop is an evidence of the formation of hard magnetic phases. However, the low value of M_s and M_r indicates that the fraction of the hard magnetic phases must be very few in these samples, and that is why such phases could not be detected by XRD analysis.

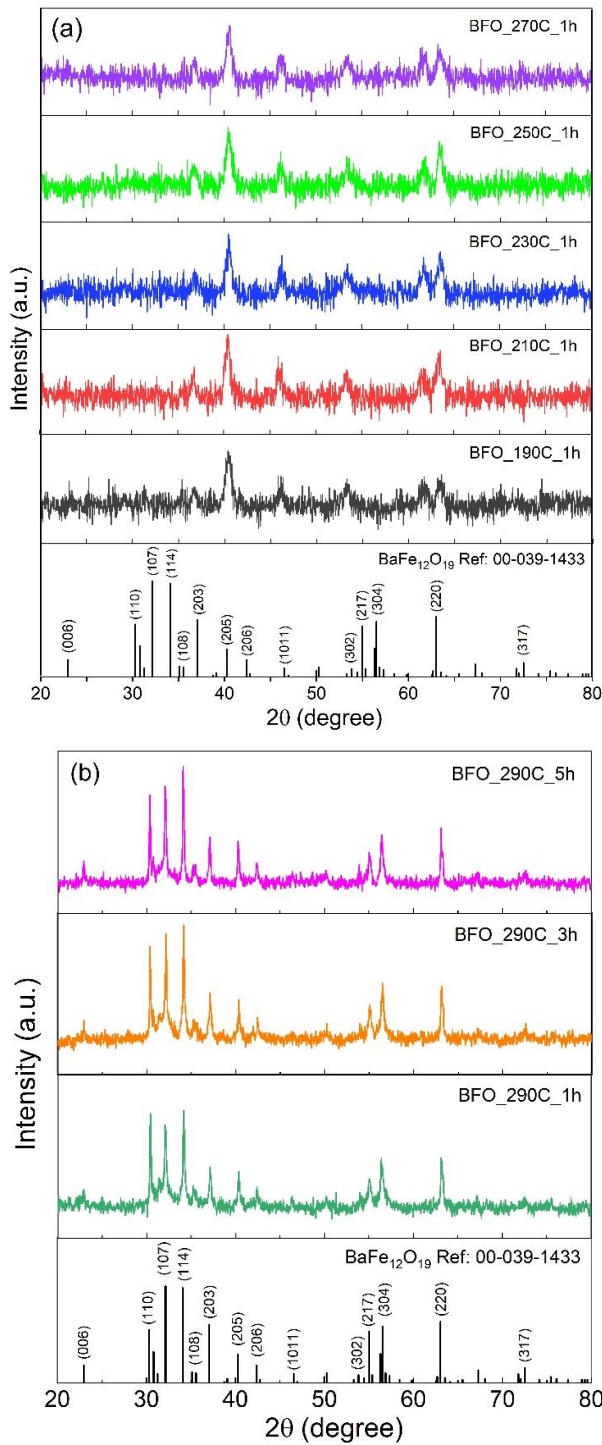


Fig. 1. The figure is center-aligned and the caption of the figure is left-aligned.

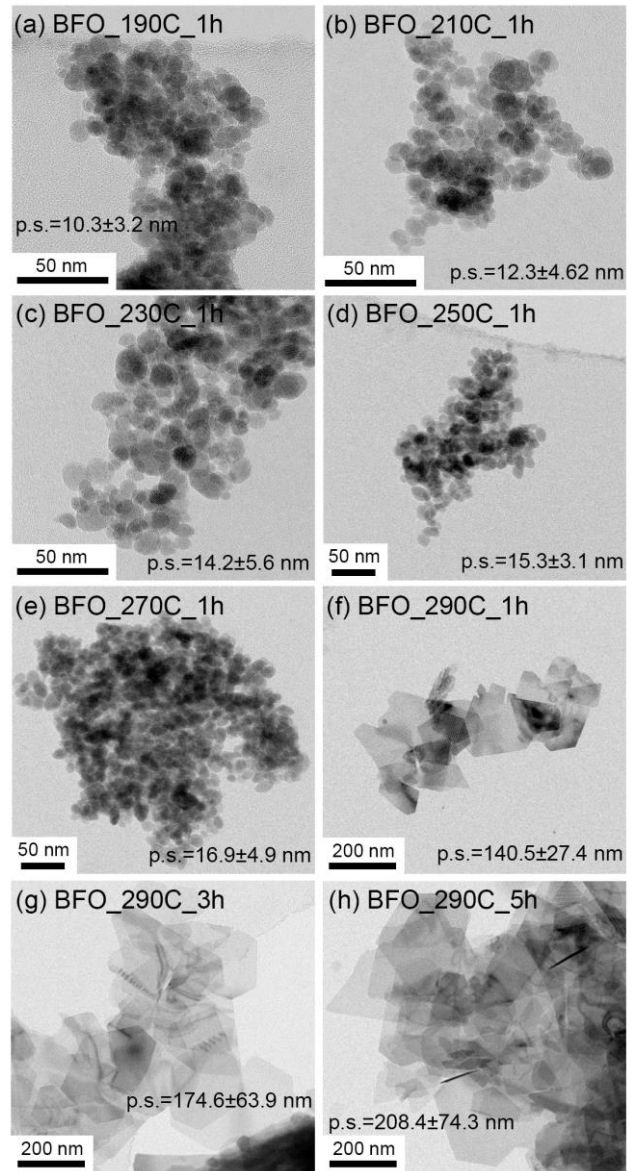


Fig. 2. TEM micrographs of the BFO NPs synthesized by hydrothermal using different temperature and time. (p.s. = particle size).

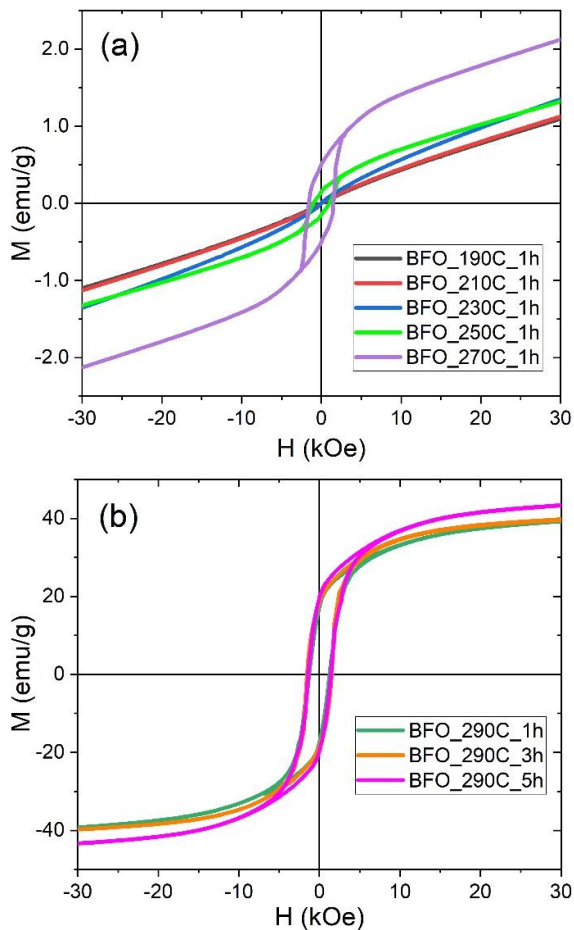


Fig. 3. VSM measurement of the BFO NPs hydrothermally synthesized at (a) different temperature (190 – 270 °C) at 1 h holding time, and (b) different holding time (1 – 5 h) at 290 °C.

Figure 3(b) shows the M-H curves of the NPs synthesized at 290 °C for 1-5 h. The clear hysteresis loops are observed in all samples, indicating the formation of the BFO phase, the hard ferromagnetic phase, as evidenced from the XRD results. The values of M_s , M_r , were enhanced significantly to around 39 – 43 emu/g, and 15 – 21 emu/g, respectively, and the H_c was found to be approximately 1.4-1.6 kOe. These values are similar to the literature values for the BFO NPs synthesized by a hydrothermal method [24, 26]. Increasing the holding time enhanced the M_s value slightly, because of the higher crystallinity and the larger size of BFO NPs as shown in XRD and TEM results, but had an insignificant effect on H_c . Compared with BFO NPs synthesized by other methods, the hard magnetic properties of BFO NPs in the present work are somewhat lower. The literatures reported the BFO NPs with M_s and H_c of 50 – 70 emu/g and 3.5 – 5.0 kOe [3, 27, 28]. However, those samples were post-annealed at high temperature above 900 °C, leading to fully formed crystalline phase and large crystallites. Thus, it is not unexpected to find the large values magnetization and coercivity for those samples.

Next, we moved to the results for the hydrothermal synthesis of the BC/BFO nanocomposites. From the previous results, we knew that the optimized conditions

for hydrothermal synthesis of BFO NPs was at 290 °C for 1-5 h. Ideally, the preparation of the BC/BFO nanocomposites should be carried out at such conditions. However, as we performed the experiments at that condition, the BC membrane was disintegrated or decomposed since it could not tolerate the temperature at 290 °C under a high-pressure condition. Hence, we had to reduce the synthesis temperature and tune the reaction time instead. The hydrothermal temperatures were varied between 150 °C and 210 °C, which is the maximum hydrothermal temperature that BC membranes can withstand, and the reaction time ranged from 1 to 7 h. The results on the structure and properties of the synthesized magnetic BC nanocomposites are discussed below.

The XRD analysis of the nanocomposites are shown in Fig. 4. For all samples, the XRD peaks of the BC phase were detected at 14.4°, 16.8°, 22.6° which are indexed to the (1 $\bar{1}$ 0), (110) and (200) planes [13, 29]. However, there are no peaks which can match with the diffraction peaks for the BFO phase, whether the samples were synthesized at different temperature 150 – 210 °C (for 1 h) or different time (at a fixed temperature of 190 °C). This result imply that the synthesis temperature and time are not sufficient to promote the BFO phase formation. It is understandable since the synthesis of NPs alone form the BFO phase only when the hydrothermal temperature was above 270 °C. This is unfortunately inevitable because it is the upper limit that the BC membrane can withstand. Increase temperature further, such as at 230 °C for 1 h, or lengthening the holding time at 190 °C more than 7 h led to the deterioration or decomposition of the BC membranes. Nevertheless, as we shall see below, even within the range of the experimental conditions, the BC/BFO nanocomposites still show hard ferromagnetic properties.

The morphology of the BC nanocomposites was investigated as shown in Fig. 5. The three-dimensional network of cellulose nanofibers is observed which was the signature of the BC structure. Each nanofiber has a diameter around 100 – 200 nm. NPs are coated uniformly on the surface of the fibers. The NPs from all synthesis conditions are very small with spherical shape, similar to the TEM observation in Fig. 2 for the NPs synthesized at lower temperature. No faceted plate-like particles are observed, implying that the BFO phase was not properly formed, as suggested by XRD. Increasing the hydrothermal temperature (from 150 to 210 °C) led to more densely packed structure since more NPs filled the pores of BC (Fig. 5(a)-(d)). Similarly, lengthening the synthesis time (from 3 to 7 h, at 190 °C) also promotes the formation of the NPs in the porous structure of BC nanofibrils (Fig. 5(e)-(g)).

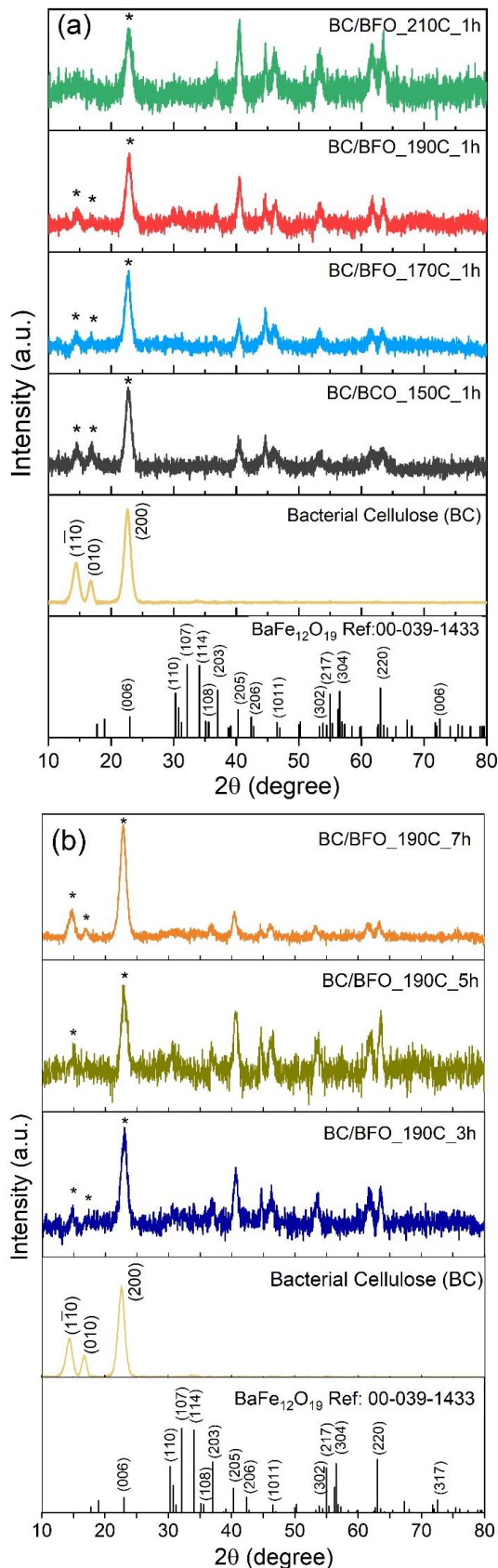


Fig. 4. XRD patterns of the BC/BFO nanocomposites hydrothermally synthesized at (a) different temperature (150 – 210 °C) at 1 h holding time, and (b) different holding time (3 – 7 h) at 190 °C.

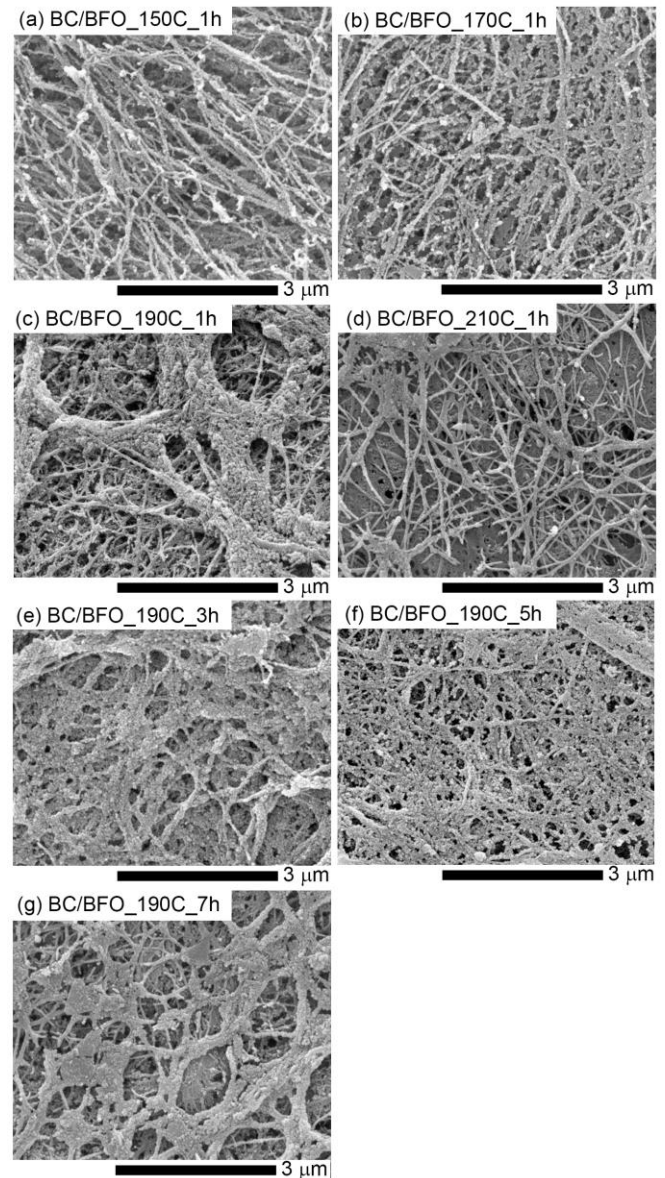


Fig. 5. SEM micrographs of the BC/BFO nanocomposites synthesized by hydrothermal using different temperature and time.

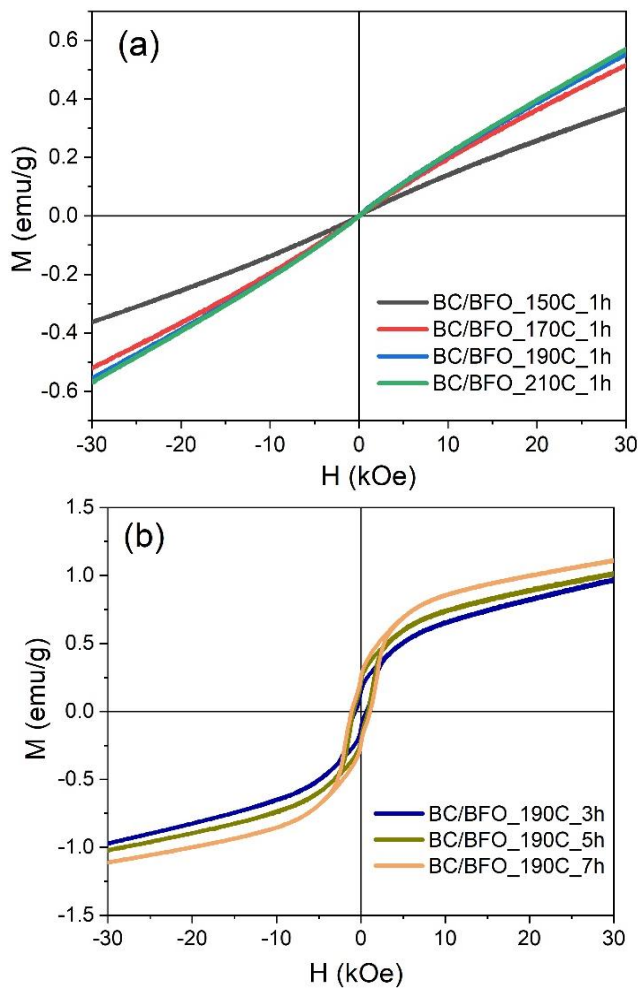


Fig. 6. VSM measurement of the BC/BFO nanocomposites hydrothermally synthesized at (a) different temperature (150 – 210 °C) at 1 h holding time, and (b) different holding time (3 – 7 h) at 190 °C.

The magnetic properties of the BC nanocomposites are shown in Fig. 6. For the samples hydrothermally synthesized for 1 h, the linear M-H curves are observed for all samples, independent of the synthesis temperature (Fig. 6(a)). This is attributed to the paramagnetic phase of the NPs since the BFO phase was not yet formed. On the other hand, the samples synthesized at 190 °C but hold for 3, 5 and 7 h showed the M-H curves with hysteresis loops (Fig. 6(b)). The size of the loops increases with longer holding times. This result is quite unexpected since there is no indication from XRD or SEM for the existence of the BFO hard magnetic phase. However, it could be argued based on the results from the previous section. In Fig. 3(a), the hysteresis loops were found for the NPs synthesized at 250 and 270 °C, even though the XRD did not detect the BFO phase. We discussed that there should exist a very small fraction of BFO NPs in the batches but could not be detected by XRD. Similar argument can apply here. Although the synthesis temperature of the BC/BFO nanocomposites was lower (only 190 °C) but the time was multiplied. Thus, the small portion of the

starting materials could be kinetically driven to form the BFO phase. Again, the existence of the BFO phase must be very few, since the M_s (0.9-1.1 emu/g) and M_r (0.2-0.3 emu/g) values are very low, as compared to the completely formed phase (M_s ~40 emu/g, Fig. 3(b)). That could be the possible reason why XRD cannot detect it.

Since hysteresis loop can be observed, it suggests that the ferromagnetic properties can be retained in the BC/BFO nanocomposites membranes. Therefore, we demonstrated the ferromagnetic behavior of the BC/BFO nanocomposites by using a permanent magnet to lift the membrane, (as shown in Fig. 7(a)). Furthermore, not only magnetically attractive, the BC/BFO nanocomposite also exhibits excellent flexibility (Fig. 7(b)). It can be bent manually and can return to its original shape after release. Moreover, it is very light. It can be placed on top of the leaves without deflecting them (Fig. 7(c)). Combining these properties (magnetically attractive, flexible, and light), the BC/BFO nanocomposites could become an interesting choice of magnetic materials. They can be exploited in several potential applications, such as information storage, anti-counterfeit, and flexible and lightweight magnets.

4. Conclusions

This work has successfully prepared BFO NPs by a hydrothermal method. The hydrothermal synthesis at 270 °C or below led to the formation of very small NPs (10 – 17 nm) but did not yield the BFO phase. Increasing the synthesis temperature to 290 °C for 1 – 5 h resulted in the NPs with the desired BFO phase. The particles exhibited the faceted plate-like shape with much larger sizes (140 – 208 nm). The NPs synthesized at low temperature showed paramagnetic property whereas increasing the synthesis temperature gradually changed the magnetic properties into superparamagnetic and ferromagnetic. The NPs synthesized at 290 °C for 5 h showed the largest hysteresis loop with M_s , M_r and H_c of 43 emu/g, 21 emu/g, and 1.6 kOe, respectively. For the hydrothermal synthesis of BC/BFO nanocomposites, the temperature range was 150 – 210 °C (for 1 h), and the time varied from 1 to 7 h (at 190 °C), which was limited by the stability of the BC membranes. Every synthesis condition could not promote the formation of the BFO phase that can be observed by XRD. In all samples, we only observed very small NPs coated on the BC nanofibers. Increasing the temperature and time led to higher deposition of NPs in the BC pores. However, magnetic hysteresis loops were observed for the nanocomposites synthesized at 190 °C for 3 – 7 h. This indicates that there might be a small fraction of BFO phase in the nanocomposite membranes but too few to be detected by XRD. The fabricated BC/BFO nanocomposite membranes were demonstrated for their magnetic attraction, flexibility, and lightness. This makes them suitable for potential uses in flexible information storage or lightweight magnets.

Acknowledgements

This work was supported by the Thailand Research Fund (TRF) in cooperation with Synchrotron Light Research Institute (public organization) and Khon Kaen University (RSA6280020), and the Basic Research Fund of Khon Kaen University.



Fig. 7. Demonstration of the BC/BFO nanocomposite for its (a) magnetic attraction, (b) flexibility, and (c) lightness.

References

- [1] B. D. Cullity and C. D. Graham, *Introduction to Magnetic Materials*, 2nd ed. Hoboken, NJ: IEEE/Wiley, 2009.
- [2] R. C. Pullar, "Hexagonal ferrites: A review of the synthesis, properties and applications of hexaferrite ceramics," *Prog. Mater. Sci.*, vol. 57, no. 7, pp. 1191-1334, 2012.
- [3] R. S. Alam, M. Moradi, M. Rostami, H. Nikmanesh, R. Moayed, and Y. Bai, "Structural, magnetic and microwave absorption properties of doped Ba-hexaferrite nanoparticles synthesized by co-precipitation method," *J. Magn. Magn. Mater.*, vol. 381, pp. 1-9, 2015.
- [4] I. Ismail, I. R. Ibrahim, K. A. Matori, Z. Awang, M. M. M. Zulkimi, F. M. Idris, R. Nazlan, R. S. Azis, M. H. M. Zaid, S. N. A. Rusly, and M. Ertugrul, "Comparative study of single- and double-layer BaFe₁₂O₁₉-Graphite nanocomposites for electromagnetic wave absorber applications," *Mater. Res. Bull.*, vol. 126, p. 110843, 2020.
- [5] H. K. Choudhary, R. Kumar, S. P. Pawar, S. Bose, and B. Sahoo, "Effect of microstructure and magnetic properties of Ba-Pb-hexaferrite particles on EMI shielding behavior of Ba-Pb-hexaferrite-polyaniline-wax nanocomposites," *J. Electron. Mater.*, vol. 49, no. 3, pp. 1618-1629, 2020.
- [6] A. Ohlan, K. Singh, A. Chandra, and S. K. Dhawan, "Microwave absorption behavior of core-shell structured poly (3,4-ethylenedioxy thiophene)-barium ferrite nanocomposites," *ACS Appl. Mater. Interfaces*, vol. 2, no. 3, pp. 927-933, 2010.
- [7] D. Klemm, B. Heublein, H. P. Fink, and A. Bohn, "Cellulose: Fascinating biopolymer and sustainable raw material," *Angew. Chem., Int. Ed.*, vol. 44, no. 22, pp. 3358-3393, 2005.
- [8] M. L. Foresti, A. Vazquez, and B. Boury, "Applications of bacterial cellulose as precursor of carbon and composites with metal oxide, metal sulfide and metal nanoparticles: A review of recent advances," *Carbohydr. Polym.*, vol. 157, pp. 447-467, 2017.
- [9] W. L. Hu, S. Y. Chen, J. X. Yang, Z. Li and H. P. Wang, "Functionalized bacterial cellulose derivatives and nanocomposites," *Carbohydr. Polym.*, vol. 101, pp. 1043-1060, 2014.
- [10] N. Shah, M. Ul-Islam, W. A. Khattak and J. K. Park, "Overview of bacterial cellulose composites: A multipurpose advanced material," *Carbohydr. Polym.*, vol. 98, no. 2, pp. 1585-1598, 2013.
- [11] N. Sriplai and S. Pinitsoontorn, "Bacterial cellulose-based magnetic nanocomposites: A review," *Carbohydr. Polym.*, vol. 254, p. 117228, 2021.
- [12] M. Chanthiwong, W. Mongkolthanasarak, S. J. Eichhorn, and S. Pinitsoontorn, "Controlling the processing of co-precipitated magnetic bacterial cellulose/iron oxide nanocomposites," *Mater. Design*, vol. 196, p. 109148, 2020.
- [13] P. Ieamviteevanich, D. Palaporn, N. Chanlek, Y. Poo-arporn, W. Mongkolthanasarak, S. J. Eichhorn, and S. Pinitsoontorn, "Carbon nanofiber aerogel/magnetic core-shell nanoparticle composites as recyclable oil sorbents," *ACS Appl. Nano Mater.*, vol. 3, pp. 3939-3950, 2020.

- [14] N. Sriplai, W. Mongkoltharuk, S. J. Eichhorn, and S. Pinitsoontorn, "Magnetic bacterial cellulose and carbon nanofiber aerogel by simple immersion and pyrolysis," *J. Mater. Sci.*, vol. 55, pp. 4113-4126, 2020.
- [15] V. Thiruvengadam and S. Vitta, "Flexible bacterial cellulose/permalloy nanocomposite xerogel sheets - Size scalable magnetic actuator-cum-electrical conductor," *AIP Adv.*, vol. 7, no. 3, p. 035107, 2017.
- [16] N. Sriplai, W. Mongkoltharuk, S. J. Eichhorn, and S. Pinitsoontorn, "Magnetically responsive and flexible bacterial cellulose membranes," *Carbohydr. Polym.*, vol. 192, pp. 251-262, 2018.
- [17] H. S. Barud, A. Tercjak, J. Gutierrez, W. R. Viali, E. S. Nunes, S. J. L. Ribeiro, M. Jafelici, M. Nalin, and R. F. C. Marques, "Biocellulose-based flexible magnetic paper," *J. Appl. Phys.*, vol. 117, no. 17, p. 17B734, 2015.
- [18] N. Sriplai, R. Mangayil, A. Pammo, V. Santala, S. Tuukkanen, and S. Pinitsoontorn, "Enhancing piezoelectric properties of bacterial cellulose films by incorporation of MnFe₂O₄ nanoparticles," *Carbohydr. Polym.*, vol. 231, p. 115730, 2020.
- [19] I. F. Nata, M. Sureshkumar, and C. K. Lee, "One-pot preparation of amine-rich magnetite/bacterial cellulose nanocomposite and its application for arsenate removal," *RSC Adv.*, vol. 1, no. 4, pp. 625-631, 2011.
- [20] H. X. Zhu, S. R. Jia, T. Wan, Y. Y. Jia, H. J. Yang, J. Li, L. Yan, and C. Zhong, "Biosynthesis of spherical Fe₃O₄/bacterial cellulose nanocomposites as adsorbents for heavy metal ions," *Carbohydr. Polym.*, vol. 86, no. 4, pp. 1558-1564, 2011.
- [21] M. Cernea, S.G. Greculeasa, R. Radu, G. Aldica, P. Ganea, V.A. Surdu, E.T. Tanasa, M. Cioangher, N. Iacob, and R.M. Costescu, "Magnetic properties of BaNi_xFe_{12-x}O₁₉ (x=0.0-1.0) hexaferrites, synthesized by citrate-gel auto-combustion and sintered by conventional and spark plasma methods," *J. Alloy Compd.*, vol. 831, p. 154850, 2020.
- [22] Y. Slimani, A. Baykal, M. Amir, N. Tashkandi, H. Gungunes, S. Guner, H. S. El Sayed, F. Aldakheel, T. A. Saleh, and A. Manikandan, "Substitution effect of Cr³⁺ on hyperfine interactions, magnetic and optical properties of Sr-hexaferrites," *Ceram. Int.*, vol. 44, no. 13, p. 15995-16004, 2018.
- [23] K. Byrappa and T. Adschiri, "Hydrothermal technology for nanotechnology," *Prog. Cryst. Growth Charact. Mater.*, vol. 53, no. 2, pp. 117-166, 2007.
- [24] Y. Liu, M. G. B. Drew, J. P. Wang, M. L. Zhang, and Y. Liu, "Efficiency and purity control in the preparation of pure and/or aluminum-doped barium ferrites by hydrothermal methods using ferrous ions as reactants," *J. Magn. Magn. Mater.*, vol. 322, no. 3, pp. 366-374, 2010.
- [25] S. Jakmuangpak, T. Prada, W. Mongkoltharuk, V. Harnchana, and S. Pinitsoontorn, "Engineering Bacterial Cellulose Films by Nanocomposite Approach and Surface Modification for Biocompatible Triboelectric Nanogenerator," *ACS Appl. Electron. Mater.*, vol. 2, no. 8, pp. 2498-2506, 2020.
- [26] D. Primc, D. Makovec, D. Lisjak, and M. Drogenik, "Hydrothermal synthesis of ultrafine barium hexaferrite nanoparticles and the preparation of their stable suspensions," *Nanotechnology*, vol. 20, no. 31, p. 315605, 2009.
- [27] I. Bsoul and S. H. Mahmood, "Magnetic and structural properties of BaFe_{12-x}GaxO₁₉ nanoparticles," *J. Alloy Compd.*, vol. 489, no. 1, pp. 110-114, 2010.
- [28] T. Ben Ghzaïel, W. Dhaoui, A. Pasko, and F. Mazaleyrat, "Effect of non-magnetic and magnetic trivalent ion substitutions on BaM-ferrite properties synthesized by hydrothermal method," *J. Alloy Compd.*, vol. 671, pp. 245-253, 2016.
- [29] N. Sriplai, P. Sirima, D. Palaporn, W. Mongkoltharuk, and S. J. Eichhorn, S. Pinitsoontorn, "White magnetic paper based on a bacterial cellulose nanocomposite," *J. Mater. Chem. C*, vol. 6, no. 42, pp. 11427-11435, 2018.



Chanagan Tanakulrungsarit was born in Khon Kaen, Thailand in 1998. She received her B.Sc. degree in Materials Science and Nanotechnology from Khon Kaen University, Thailand in 2020. She is now self-employed for her own business.



Wiyada Mongkolthanaruk, Ph.D (Molecular biology and biotechnology) from Sheffield University. She is currently an Assistant Professor in Department of Microbiology, Faculty of Science, Khon Kaen University. Her research interests include functions of endophytic bacteria for plant growth promotion in stress conditions, gene expression involved in inulin/fructan production and GABA enhancement in rice seeds from bacteria.



Sampo Tuukkanen received his Ph.D. in Applied physics from Department of Physics, University of Jyväskylä, Finland, in 2006. He is currently working as Associate Professor (tenure track) at Tampere University, Finland. His research interests are biomeasurements and bio-based devices. He has authored over 60 articles and has an h-index of 21.



Supree Pinitsoontorn received his D.Phil in Materials from Department of Materials, University of Oxford, UK, in 2008. He is currently working as an Associate Professor in Physics at Khon Kaen University, Thailand. His research interests include thermoelectric materials, magnetic nanoparticles, and bacterial cellulose nanocomposites. He has authored over 100 articles and has an h-index of 20.